Supplement for:

Kinetics, SOA yields and chemical composition of secondary organic aerosol from β-caryophyllene ozonolysis with and without nitrogen oxides between 213 and 313 K

Linyu Gao[1,2*], Junwei Song[1,2], Claudia Mohr[3], Wei Huang[4], Magdalena Vallon[1], Feng Jiang[1,2], Thomas Leisner[1,5], and Harald Saathoff[1*]

1. Institute of Meteorology and Climate Research, Karlsruhe Institute of Technology, Karlsruhe, Germany
2. Institute of Geography and Geoecology, Working Group for Environmental Mineralogy and Environmental System Analysis, Karlsruhe Institute of Technology, Karlsruhe, Germany
3. Department of Environmental Science, Stockholm University, Stockholm, Sweden
4. Institute for Atmospheric and Earth System Research / Physics, Faculty of Science, University of Helsinki, Helsinki, Finland
5. Institute of Environmental Physics, Heidelberg University, Heidelberg, Germany

Correspondence to: Linyu Gao (linyu.gao@kit.edu) and Harald Saathoff (harald.saathoff@kit.edu)
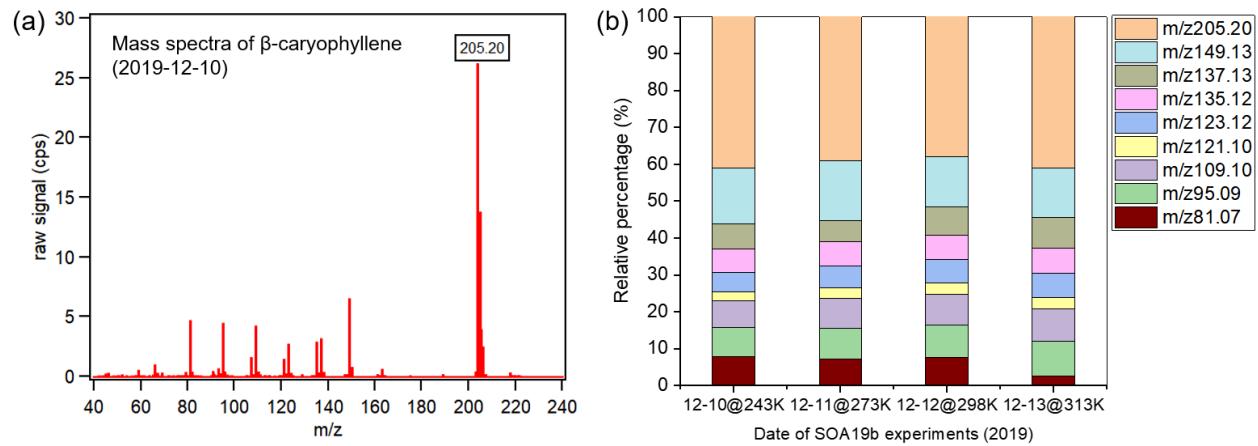
Figure S1. (a) Example of the 5-min average mass spectra of β-caryophyllene subtracted from the chamber background when the β-caryophyllene ion (*m/z* 205.20) shows relatively stable signal intensity in the chamber and (b) relative contribution of β-caryophyllene related ions detected by the PTR-MS in this study.
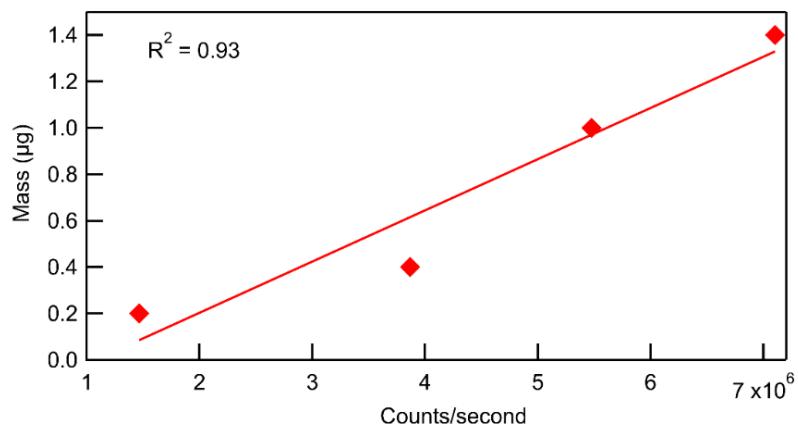
Figure S2: Calibration of the FIGAERO-CIMS with the β-caryophyllinic acid (BCA). The β-caryophyllinic acid was dissolved into methanol to 0.2 ng m⁻³ as a standard BCA solution. Different volume of the standard BCA solution was deposited on a PTFE filter and then the deposited filter was heated by FIGAERO -CIMS carried by ultra-high purity nitrogen following a thermal desorption, as described in Section 2.1. The sensitivity of CIMS to β-caryophyllinic acid was calculated as $\left(2.4^{+0.96}_{-0.63}\right)$ cps ppt⁻¹.
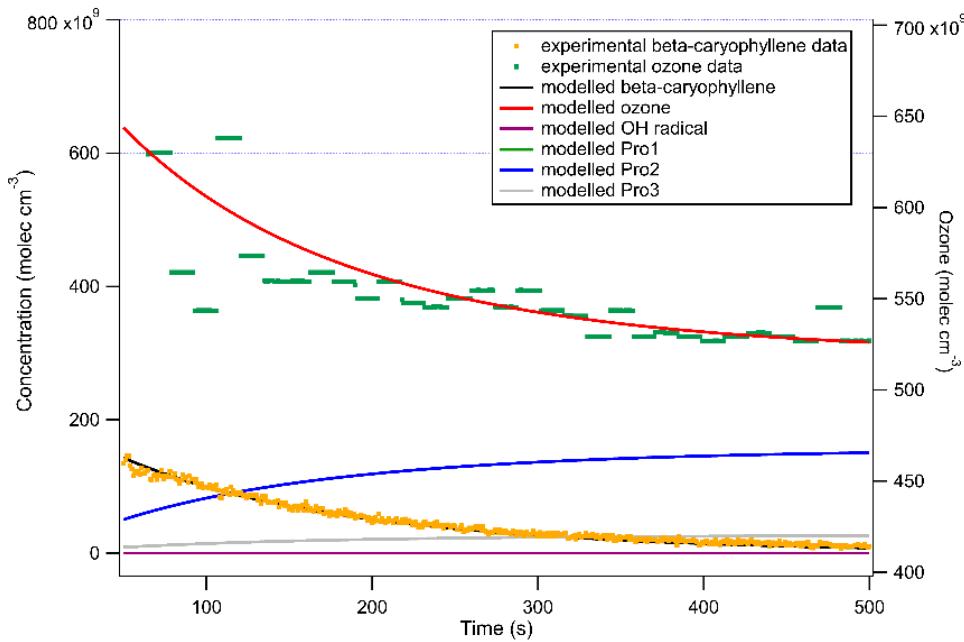
Figure S3: Example of the fit of the kinetic model to the observation for the experiment at 313K. Three main reactions were considered in the kinetic analysis to fit the observations:

Reaction1: BCP + O$_3$ → Pro1 + OH, k_1;

Reaction2: BCP + O$_3$ → Pro2, k_2;

Reaction3: BCP + OH → Pro3, k_3

where BCP is the beta-caryophyllene, Pro1, Pro2 and Pro3 represent different reaction products, and k_1, k_2, k_3 the corresponding reaction rate constants.
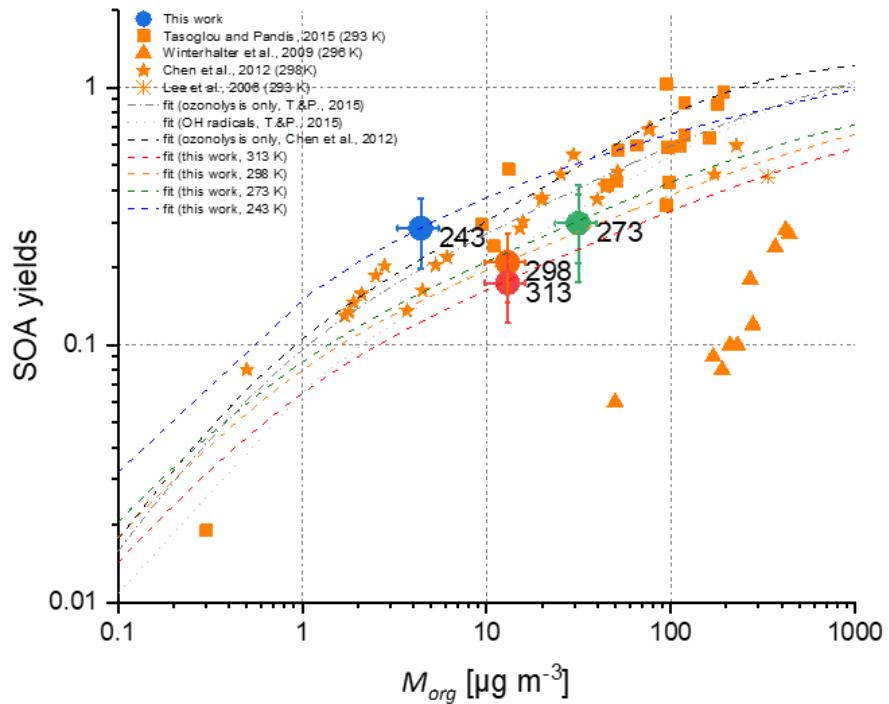
Figure S4: Temperature dependence of SOA yields as a function of the total organic particle mass concentration (M_{org}). Fitted lines are based on volatility distributions.
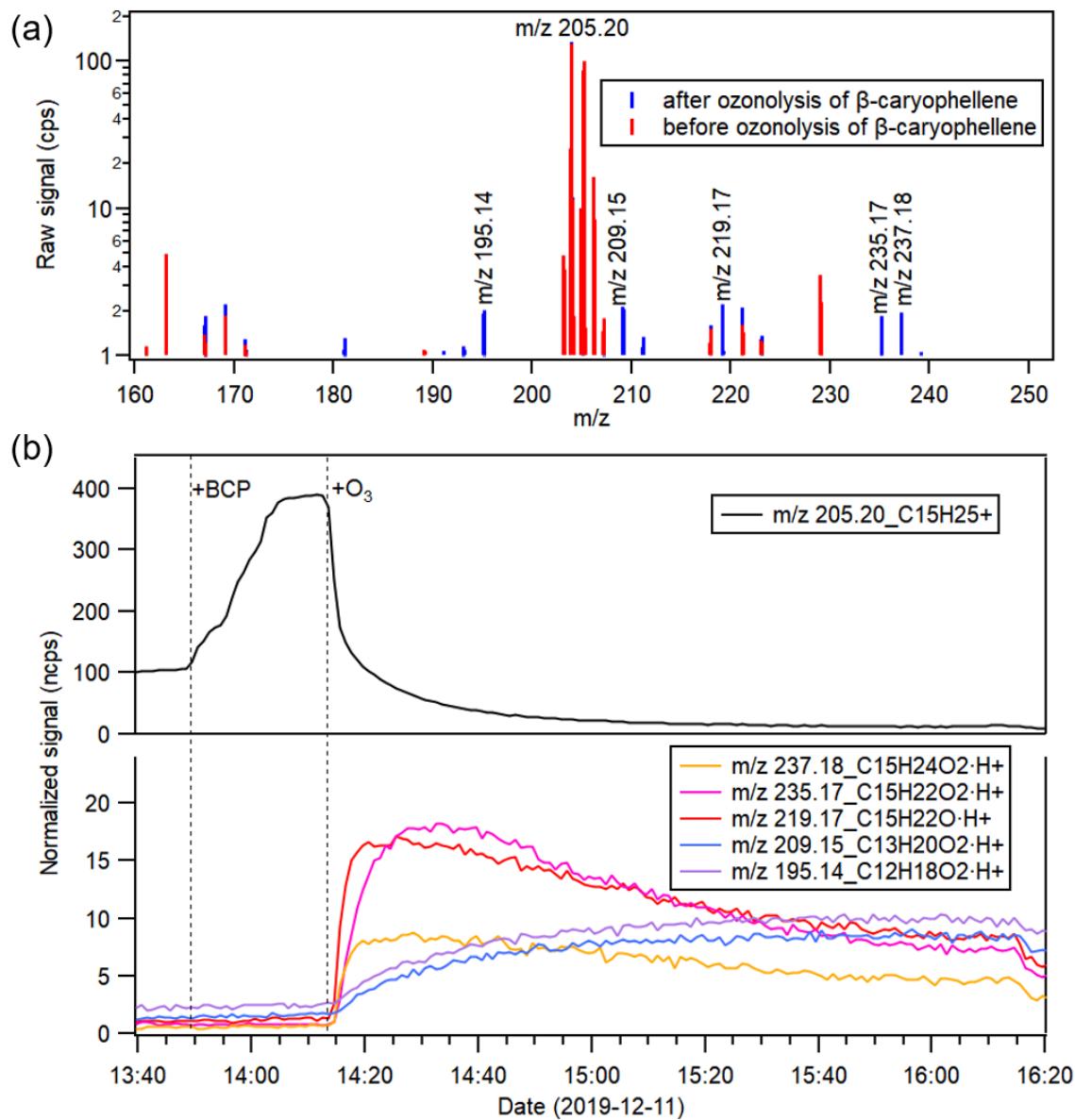
Figure S5: (a) Comparison between the average mass spectra detected by the PTR-MS over the 5 min before and after ozonolysis of β-caryophyllene in the experiment at 273 K on 12/11/2019. **(b)** Time series of β-caryophyllene (*m/z* 205.20) and several major gas phase product ions (*m/z* 237.18, *m/z* 235.17, *m/z* 219.17, *m/z* 209.15 and *m/z* 195.14) as labelled in (a). Two dashed line show the time points of β-caryophyllene addition and first O₃ addition to the chamber, respectively.
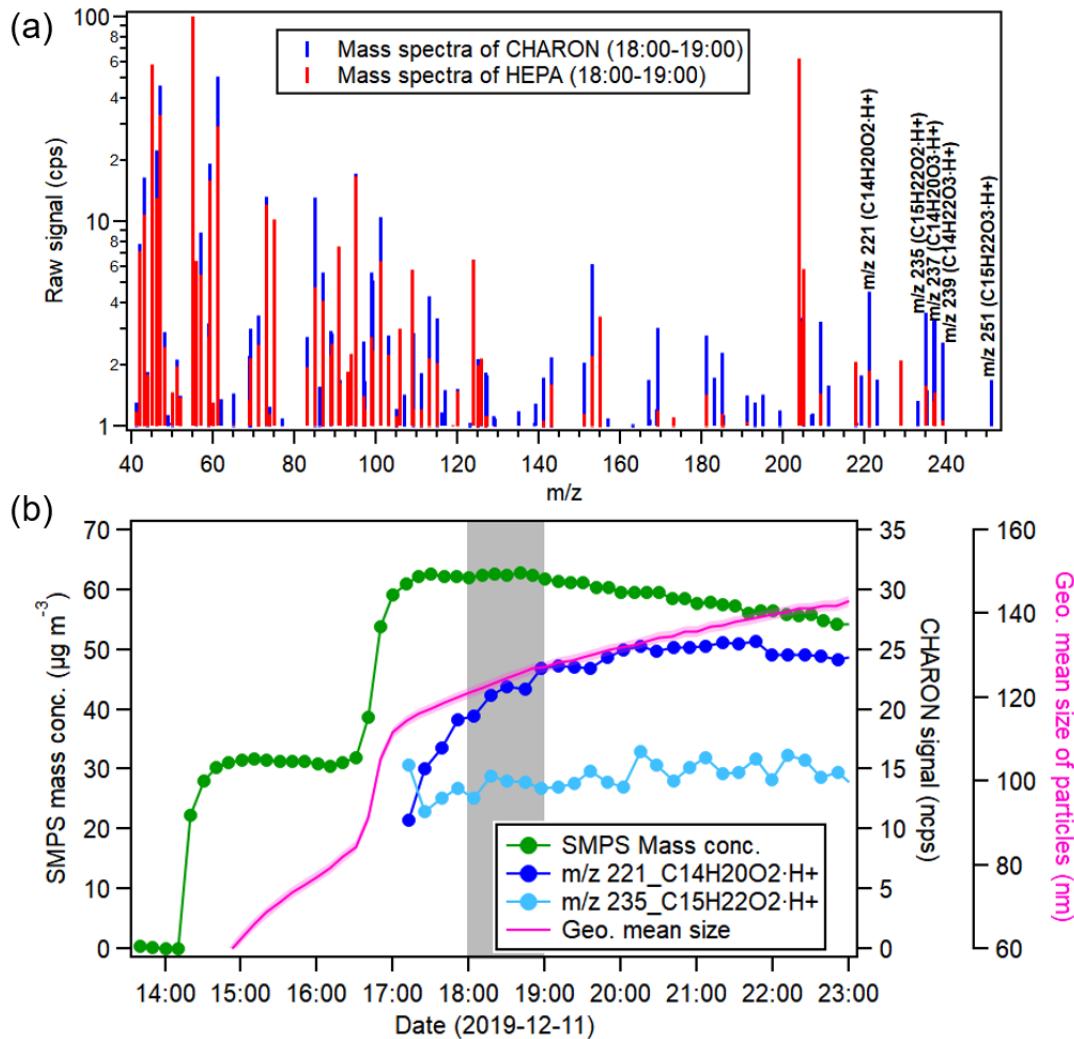
Figure S6: (a) Average mass spectra of particle phase by the CHARON (blue) and HEPA filter (red) measurement over the course of 1 hour (18:00-19:00 as shown in gray area in (b), aerosol mass concentration: 62 ± 0.3 μg m⁻³) in the β-caryophyllene ozonolysis experiment at 273 K in 12/11/2019. Several major product ions (*m/z* 221, 235, 237, 239 and 251) are labelled. **(b)** time series of SMPS mass concentration of aerosol particles and two particle phase product ions (*m/z* 221 and 235) detected by the CHARON-PTR-MS. The time series of geometric mean size of aerosol particles is given to show the reduced transmission efficiency of CHARON inlet for smaller particles.
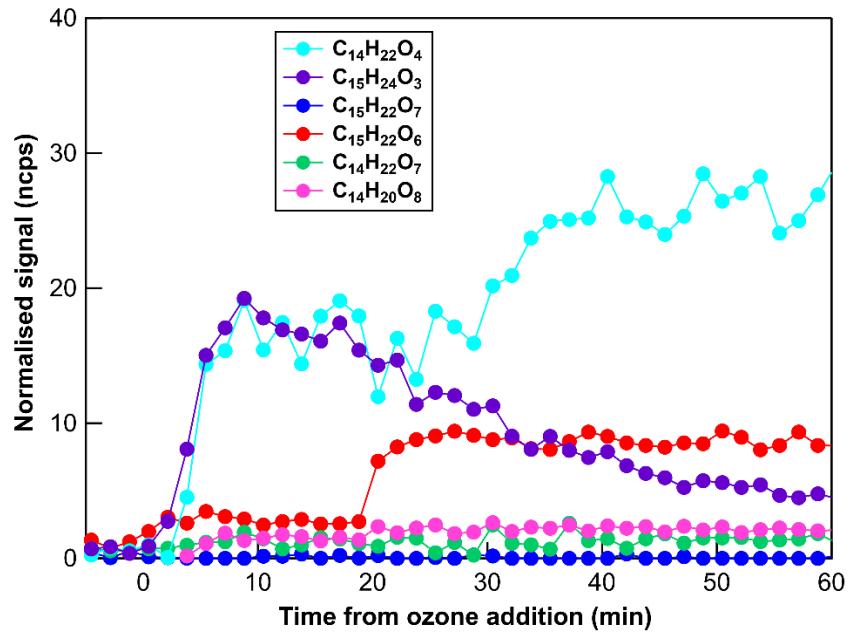
Figure S7. Evolution of major oxidation products detected by CIMS in the gas phase in the absence of NO₂. The time zero represents the timepoint when ozone was added first.
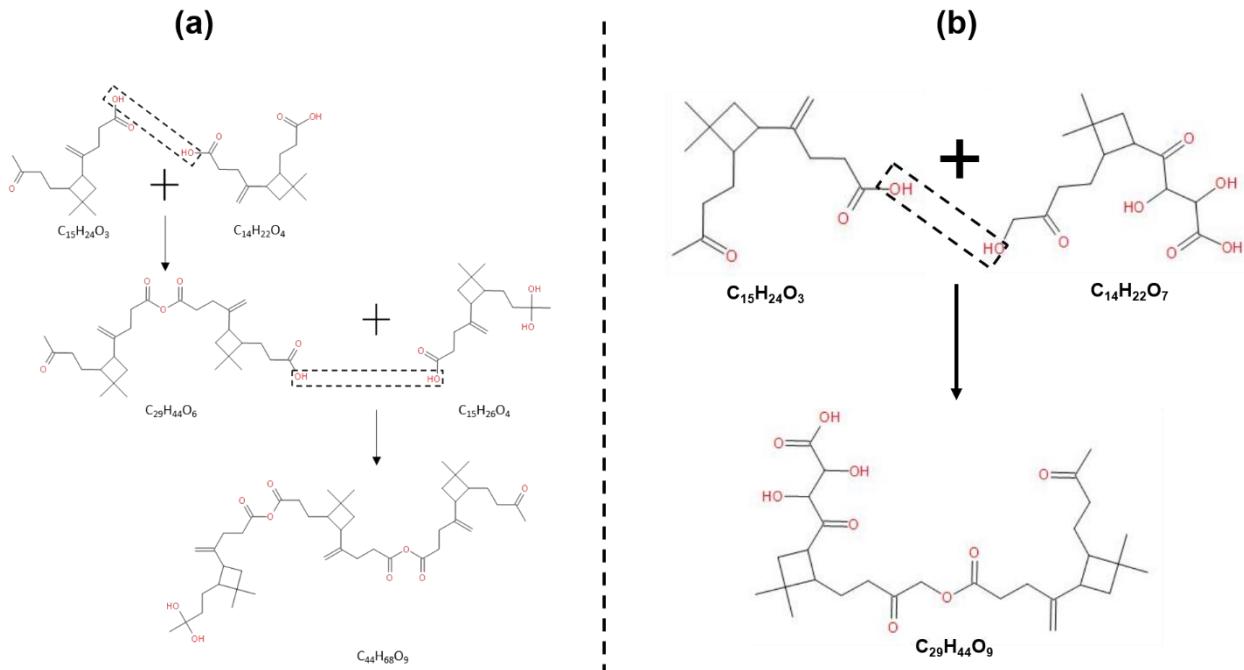
Figure S8. The potential esterification pathways of the formation of C$_{29}$ and C$_{44}$ compounds at 213 K. The structure of C$_{15}$H$_{24}$O$_3$, C$_{14}$H$_{22}$O$_4$, C$_{15}$H$_{26}$O$_4$, and C$_{14}$H$_{22}$O$_7$ were identified by (Li et al., 2011; Chan et al., 2011). Panel (a) shows the dimer (C$_{29}$H$_{44}$O$_6$) and trimer (C$_{44}$H$_{68}$O$_9$) formation at 213K; panel (b) represents the dimer (C$_{29}$H$_{44}$O$_9$) at 313K.

Similarly, the formation pathway of C30 and C35 compounds could be speculated as follows:

213K: $C_{15}H_{24}O_3 + C_{15}H_{26}O_3 \rightarrow C_{30}H_{48}O_5 + H_2O$

$\qquad C_{30}H_{48}O_5 + C_{14}H_{22}O_5 \rightarrow C_{44}H_{68}O_9 + H_2O$

313K: $C_{15}H_{24}O_4 + C_{20}H_{26}O_9 \rightarrow C_{35}H_{48}O_{12} + H_2O$

$\qquad C_{15}H_{24}O_4 + C_{15}H_{22}O_5 = C_{30}H_{44}O_8 + H_2O$

$\qquad C_{30}H_{44}O_8 + C_5H_7O_6N = C_{35}H_{49}O_{13}N + H_2O$
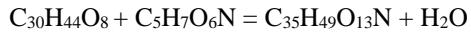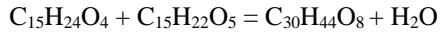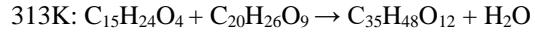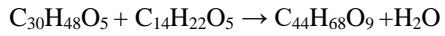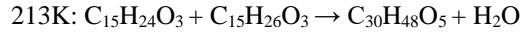
Note that we observed a short but significant increase of the dimer signal $C_{30}H_{48}O_5$ in the gas phase at 213K after the second addition of β-caryophyllene into the chamber. This suggests that the dimer formation could happen in the gas phase at 213K. However, no significant signal change of dimeric molecules was observed at 313K in the gas phase over the course of the experiments. One explanation could be the dimeric compounds (e.g. $C_{29}H_{44}O_9$) are quite highly oxygenated and extremely low volatile, resulting in a fast condensation process before being detected in the gas phase. The possibility cannot be excluded that the dimeric compounds could be formed in the condensed phase as no dimeric signals could be detected visibly even with the time resolution of 1 s.
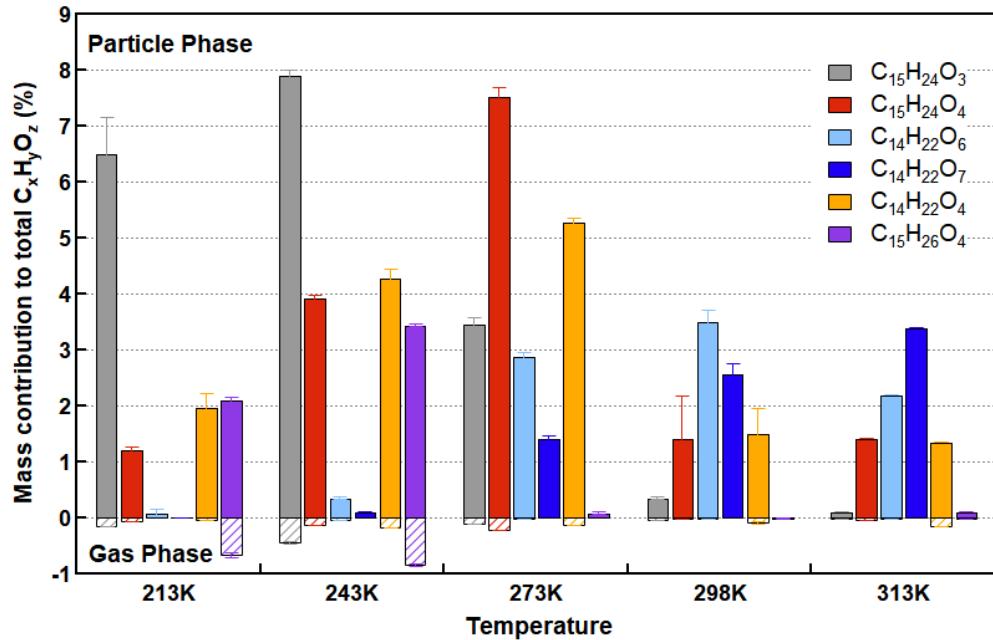
Figure S9. Fractions of six major particle phase compounds to the sum of all CxHyOz compounds as a function of temperature. The particle fraction (solid bars) and the gas fraction (dashed bars) of each compound are shown.

Figure S9 shows the temperature dependent fractions of six typical and most abundant monomers including the β-caryophyllene tracer, β-caryophyllinic acid ($C_{14}H_{22}O_4$), in both gas and particle phase as formed from β-caryophyllene ozonolysis without NO_2. Among the few compounds in the gas phase, $C_{15}H_{26}O_4$ and $C_{15}H_{24}O_3$ (likely β-caryophyllonic acid) contributed mainly at lower temperatures (213 – 243 K). $C_{14}H_{22}O_4$ was observed at all temperatures even though its contribution was on average only 0.05% to the total mass including gas and particle phase. In the particle phase, $C_{15}H_{24}O_4$ (likely β-hydroxycaryophyllonic acid) was observed at all temperatures and contributed most at 273 K. $C_{15}H_{24}O_3$ and $C_{15}H_{26}O_4$ were mainly present at lower temperatures. The two most abundant auto oxidation products, $C_{14}H_{22}O_6$ (likely hydrated β-oxocaryophyllonic acid) and $C_{14}H_{22}O_7$ (not yet identified) were observed at all temperatures but their signals were significantly increasing with temperature. Their mass contribution in the particle phase were 0.08 to 2.3% and 0.01 to 3.6% from 213 K to 313 K, respectively.
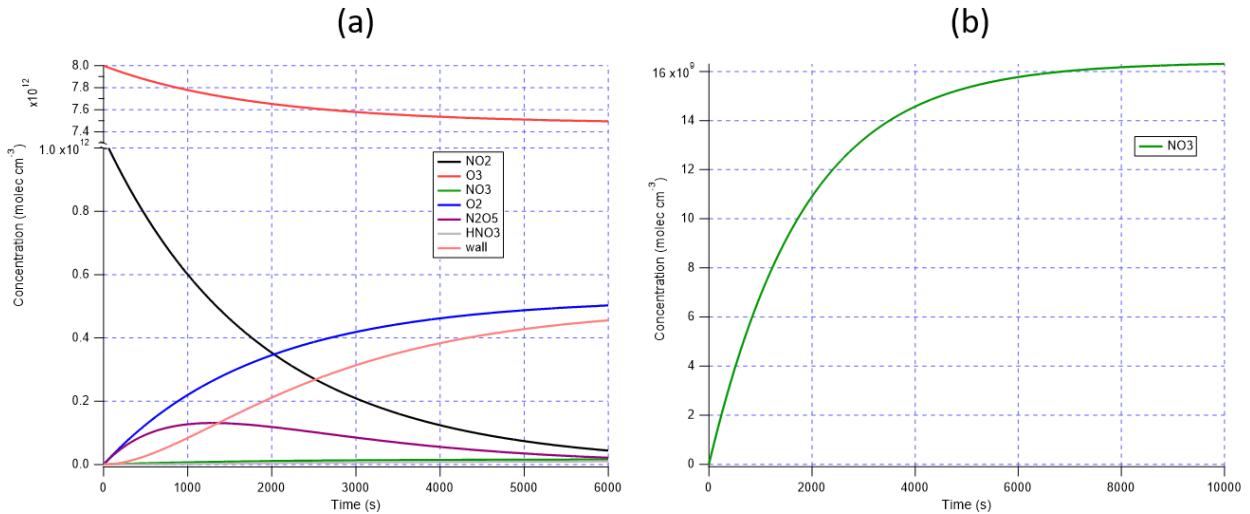
Figure S10. Modelling the NO₃ radical formation at 298K before the last β-caryophyllene addition. Time evolution of all reactants are modelled (left panel), including NO₂ (black line), O₃ (red line), NO₃ (green line), O₃ (blue line), N₂O₅ (purple line), HNO₃ (grey line) and wall loss (orange line). The right panel shows the NO₃ concentration evolution alone. Time zero is marked as the start of NO₂ addition.

Because of an excess of ozone in the chamber over the course of the whole experiment, the following reactions were considered:

$NO_2 + O_3 \rightarrow NO_3 + O_2$,   k1

$NO_3 + NO_2 \rightarrow N_2O_5$,   k2

$N_2O_5 \rightarrow NO_2 + NO_3$,   k3

$N_2O_5 + H_2O \rightarrow HNO_3$,   k4

$N_2O_5 \rightarrow wall$,   k5
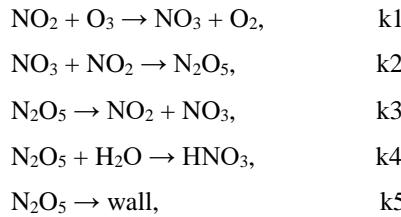
All the rate constants used at all temperatures are listed below (IUPAC Task Group on Atmospheric Chemical Kinetic Data Evaluation (ipsl.fr), https://iupac-aeris.ipsl.fr/#):

	k1	k2	k3	k4	k5*
213K	1.3E-18	3.5E-10	8.3E-07	1.00E-22	1.00E-03
243K	5.4E-18	2.0E-10	5.5E-04	1.00E-22	1.00E-03
273K	1.6E-17	1.3E-10	0.09	1.00E-22	1.00E-03
298K	3.5E-17	8.9E-11	2.9	1.00E-22	1.00E-03
313K	5.2E-17	7.3E-11	17.8	1.00E-22	1.00E-03

*Estimated from previous experiments with N2O5 measured inside the AIDA chamber by FTIR.
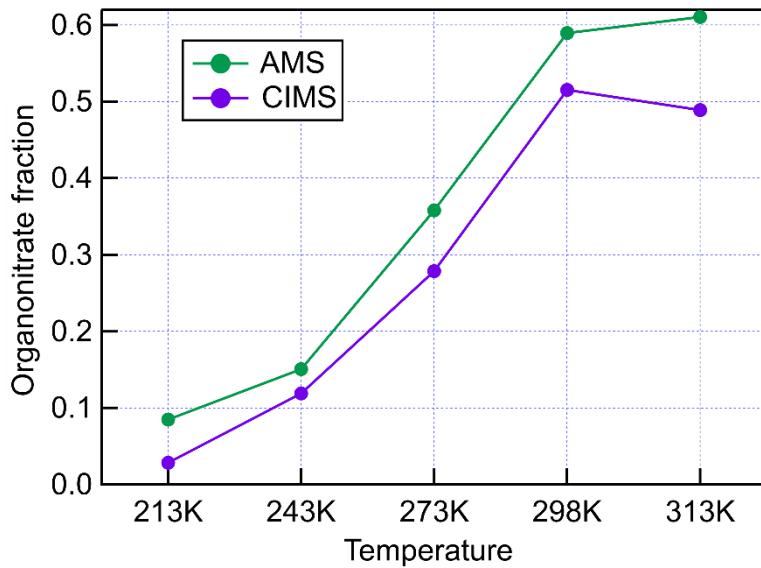
Figure S11. Comparison of the temperature dependence on the organonitrate fraction formed. The green dots represent the fraction of the organonitrate concentrated detected by HR-AMS, while the blue dots show the signal fraction of organonitrate assigned by FIGAERO-iodide-CIMS.
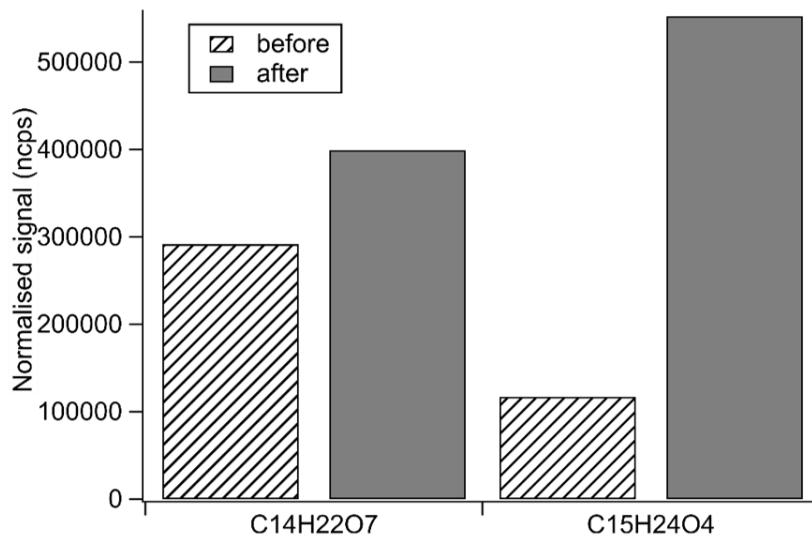
Figure S12. Comparison of the CIMS signals of $C_{14}H_{22}O_7$ and $C_{15}H_{24}O_4$ before (dashed) and after (solid) the last β-caryophyllene addition.
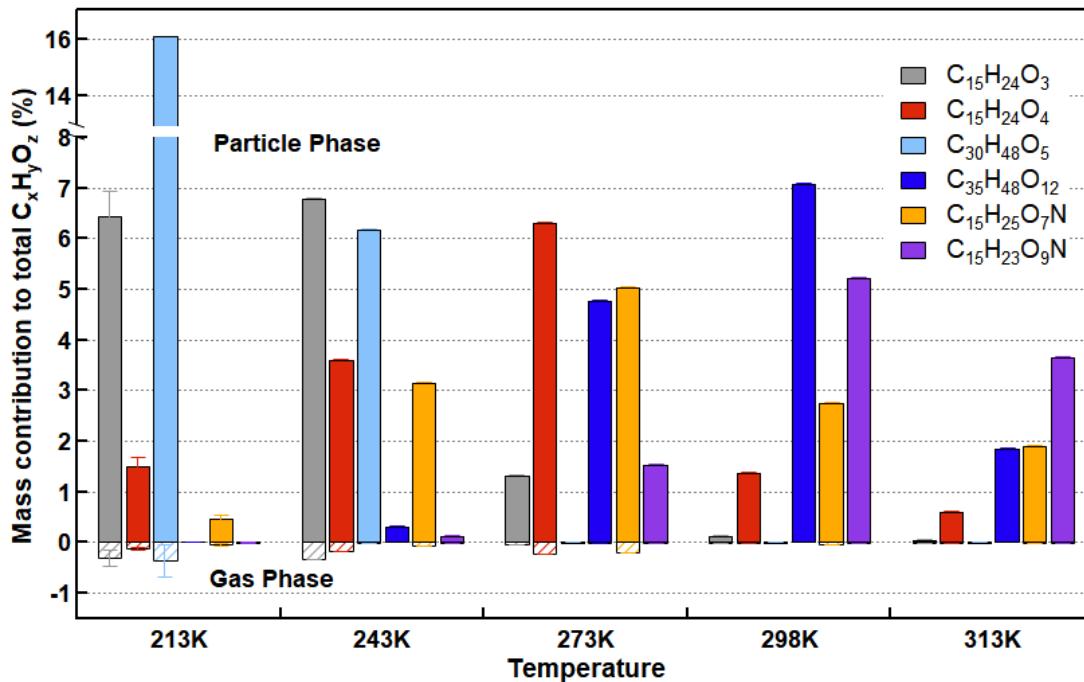
Figure S13. Mass fractions of major particle phase compounds to the sum of all detected molecues as a function of temperature. The particle fraction (solid bars in the top) and the gas fraction (dashed bars in the bottom) of each compound are shown.

As shown in Fig S13, compared to the case in the absence of NO_2, the mass fraction of $C_{15}H_{24}O_3$ and $C_{15}H_{24}O_4$ decreased in both gas and particle phase. $C_{30}H_{48}O_5$ contributed more at low temperatures (213 – 243 K) in particle and a relatively large portion of its gas signal showed at the coldest experiment (213 K), which indicates the vapor pressure of $C_{30}H_{48}O_5$ was not so low enough to condense to the particle phase completely even though it had a long carbon skeleton and high mass weight. In contrast, $C_{35}H_{48}O_{12}$ had stronger signals at high temperatures (273 – 313 K). However, nearly no gas signal could be detected under all temperatures due to its highly oxidation degree, indicative of those compounds to be extremely low volatile components, such as $C_{30}H_{48}O_5$ and $C_{15}H_{23}O_9N$. In addition, $C_{15}H_{25}O_7N$ acted as another most abundant nitrated compounds showed highest mass fraction at 273 K in both gas and particle phase.

Table S1. Compilation of experimental conditions and particle mass yields reported in the literature for β-caryophyllene ozonolysis

Reference	Temperature [K]	ΔM_{org} [µg m^{-3}]	RH [%]	Scavenger for OH or CI	Seed	Yield [%]
(Tasoglou and Pandis, 2015)	293	0.3-194	<10	2-butanol	None	1.9-104
Winterhalter et al. (2009)	296	50-370	dry	none	None	6-24
Jaoui et al. (2003)	287-290	-	80-85	none	None	39
Lee et al. (2006a)	293	336 ± 3	6.2	Cyclohexane	None	45 ± 2
Lee et al. (2006b)	295	212	56	None	None	68
Chen et al. (2012)	298	0.5-230	40	Cyclohexane	AS	8-70

For the ozonolysis of β-caryophyllene without OH scavenger, a SOA mass yield of 27% was observed at 293 K and an organic particle mass loading of 10 µg m^{-3} (Tasoglou and Pandis, 2015). Winterhalter et al. (2009) measured yields ranging between 5 - 24% for particle mass loadings of 50 - 440 µg m^{-3} and no Criegee intermediate scavenger, with the yields increasing for higher concentrations of water vapour or formic acid. Jaoui et al. (2003) measured a yield of 39.3 % without OH scavenger at 287-290 K and Lee et al. (2006a) observed a yield of 45% at 293K and a particle mass loading of 336 µg m^{-3} using cyclohexane as OH scavenger. Chen et al. (2012b) varied the ozone levels and determined SOA yields between 8 - 46% for organic particle masses of 0.5-170 µg m^{-3}, 15.8-60% at 2.1 - 230 µg m^{-3}, and 14.6-69.5% at 19 - 77.4 µg m^{-3} for ozone levels of 50 ppb, 100 ppb and 200 ppb, respectively. By using OH scavenger, Tasoglou and Pandis (2015) also quantified SOA mass yields at room temperature to be 64.4% at 17.6 µg m^{-3} for 300 ppb of ozone, 59.6% at 16.3 µg m^{-3} for 400 ppb of ozone, and 66.9% at 30.5 µg m^{-3} for 500 ppb of ozone.

Table S2. Fitted reaction rates k_{O_3} and OH radical yields for temperatures between 243K to 313K

Temperature [K]	k_{O_3} [cm^3 molecule^{-1} s^{-1}]	OH yields
313	(1.01±0.09) E-14	0.15±0.02
298	(1.09±0.21) E-14	0.08±0.01
258	(1.05±0.25) E-14	0.05±0.03
243	(1.99±0.28) E-14	0.05±0.02

Table S3. Main β-caryophyllene oxidation products and their phase partitioning

Formula	m/z (Th)	Compound assignment from literature	Ref.	Potential dimer
C2-C4 fragments				
$C_4H_6O_4$	118.0			
$C_2H_4O_3$	76.0			
C14-15 monomers				
$C_{14}H_{22}O_3$	238.2	β-nocaryophyllon aldehyde	a, b, c, d	
$C_{15}H_{24}O_3$	252.2	β-hydroxycaryophyllon aldehyde; β-caryophyllonic acid	a, b, c, d	$C_{30}H_{48}O_6$
$C_{14}H_{22}O_4$	254.2	β-hydroxynocaryophyllon aldehyde; β-nocaryophyllonic acid; β-caryophyllinic acid	a, b, c, d	$C_{28}H_{44}O_8$
$C_{15}H_{24}O_4$	268.2	β-hydroxycaryophyllonic acid	a, d	
$C_{15}H_{26}O_4$	270.2	Hydrated β-caryophyllonic acid	a	
$C_{14}H_{22}O_6$	286.1	Hydrated β-oxocaryophyllonic acid	a	$C_{28}H_{44}O_{12}$
$C_{14}H_{22}O_7$	302.1		b	
$C_{14}H_{24}O_7$	304.2			
$C_{15}H_{26}O_5$	286.2	Hydrated β-hydroxycaryophyllonic acid	a	$C_{30}H_{52}O_{10}$
$C_{15}H_{22}O_6$	298.1			
$C_{15}H_{22}O_7$	314.1		a	
$C_{14}H_{20}O_8$	316.1			
$C_{14}H_{22}O_8$	318.1			
$C_{15}H_{22}O_8$	330.1			
$C_{14}H_{22}O_9$	334.1			
$C_{15}H_{24}O_9$	348.1			
$C_{15}H_{30}O_9$	354.2			
$C_{15}H_{25}NO_8$	347.2		a	$C_{30}H_{50}N_2O_{16}$
$C_{14}H_{23}NO_9$	349.1		a	$C_{28}H_{46}N_2O_{18}$
$C_{15}H_{27}NO_8$	349.2		a	
$C_{15}H_{25}NO_9$	363.2		a	$C_{30}H_{50}N_2O_{18}$
C28-30 dimers				
$C_{28}H_{44}O_5$	460.3			
$C_{30}H_{48}O_5$	488.3			
$C_{29}H_{46}O_6$	490.3			
$C_{28}H_{44}O_7$	492.3			
$C_{30}H_{48}O_6$	504.3			
$C_{29}H_{46}O_7$	506.3			
$C_{28}H_{44}O_8$	504.3			
$C_{30}H_{48}O_7$	520.3			
$C_{29}H_{46}O_8$	552.3			
$C_{30}H_{48}O_8$	536.3			
$C_{29}H_{44}O_9$	536.3			
$C_{29}H_{46}O_9$	538.3			
$C_{29}H_{44}O_{10}$	552.3			
$C_{28}H_{42}O_{11}$	554.3			
$C_{29}H_{44}O_{11}$	568.3			
Others				
$C_{11}H_{18}O_3$	198.1	3,3-dimethyl-2-(3-oxobutyl)cyclobutanecarboxylic acid	b	
$C_{13}H_{20}O_5$	256.1	β-hydroxynornocaryophyllonic acid	a	$C_{26}H_{40}O_{10}$
$C_{35}H_{48}O_{12}$	660.3			
$C_{44}H_{68}O_9$	740.5			

[a] (Chan et al., 2011); [b] (Li et al., 2011); [c] (Winterhalter et al., 2009); [d] (Jaoui et al., 2003)

Reference

Chan, M., Surratt, J., Chan, A., Schilling, K., Offenberg, J., Lewandowski, M., Edney, E., Kleindienst, T., Jaoui, M., and Edgerton, E.: Influence of aerosol acidity on the chemical composition of secondary organic aerosol from β-caryophyllene, Atmospheric Chemistry and Physics, 11, 1735-1751, 2011.

Chen, Q., Li, Y. L., McKinney, K. A., Kuwata, M., and Martin, S. T.: Particle mass yield from *β*-caryophyllene ozonolysis, Atmos. Chem. Phys., 12, 3165-3179, 10.5194/acp-12-3165-2012, 2012.

Jaoui, M., Leungsakul, S., and Kamens, R. M.: Gas and Particle Products Distribution from the Reaction of β-Caryophyllene with Ozone, Journal of Atmospheric Chemistry, 45, 261-287, 10.1023/A:1024263430285, 2003.

Lee, A., Goldstein, A. H., Keywood, M. D., Gao, S., Varutbangkul, V., Bahreini, R., Ng, N. L., Flagan, R. C., and Seinfeld, J. H.: Gas-phase products and secondary aerosol yields from the ozonolysis of ten different terpenes, Journal of Geophysical Research: Atmospheres, 111, https://doi.org/10.1029/2005JD006437, 2006a.

Lee, A., Goldstein, A. H., Kroll, J. H., Ng, N. L., Varutbangkul, V., Flagan, R. C., and Seinfeld, J. H.: Gas-phase products and secondary aerosol yields from the photooxidation of 16 different terpenes, Journal of Geophysical Research: Atmospheres, 111, https://doi.org/10.1029/2006JD007050, 2006b.

Li, Y., Chen, Q., Guzman, M., Chan, C. K., and Martin, S.: Second-generation products contribute substantially to the particle-phase organic material produced by [beta]-caryophyllene ozonolysis, Atmospheric Chemistry and Physics, 11, 121, 2011.

Tasoglou, A., and Pandis, S.: Formation and chemical aging of secondary organic aerosol during the β-caryophyllene oxidation, Atmospheric Chemistry & Physics, 15, 2015.

Winterhalter, R., Herrmann, F., Kanawati, B., Nguyen, T. L., Peeters, J., Vereecken, L., and Moortgat, G. K.: The gas-phase ozonolysis of β-caryophyllene (C 15 H 24). Part I: an experimental study, Physical Chemistry Chemical Physics, 11, 4152-4172, 2009.